TOMOGRAPHY® RESEARCH ARTICLE

Quantitative Analysis of the Spatial Distribution of Metastatic Brain Lesions

Ted K. Yanagihara[1], Albert Lee[1], and Tony J. C. Wang[1,2]

[1]Department of Radiation Oncology and [2]Herbert Irving Comprehensive Cancer Center, Columbia University Medical Center, New York, New York

Corresponding Author:
Ted K. Yanagihara, MD, PhD
Department of Radiation Oncology, Columbia University Medical Center, 622 West 168th St., CHONY Basement North Room B11;
E-mail: tky2102@columbia.edu

Key Words: brain metastases, MRI, breast cancer, lung cancer

Abbreviations: Brain metastases (BMs), whole-brain radiotherapy (WBRT), magnetic resonance imaging (MRI), intensity-modulated radiation therapy (IMRT), Montreal Neurological Institute (MNI), regions of interest (ROIs)

ABSTRACT

Brain metastases (BMs) are the most common intracranial malignancy and afflict ~10%–20% of patients with cancer. BMs tend to present at the boundaries of gray and white matter because of the distribution of small vessels. In addition, metastases may not be randomly distributed across gross anatomical regions of the brain, but this has not previously been quantified. We retrospectively analyzed a series of 28 patients with recurrent BMs with a total of 150 lesions. Each lesion was manually defined based on T1 gadolinium-enhanced imaging. Standard brain atlases were used to identify the anatomical brain region affected by each BM and the frequency of metastases in each region was compared with the expected probability, which was assumed to be a random distribution based on the brain volume. After correction for multiple comparisons, the paracingulate gyrus was found to have a statistically significant increase ($P = 4.731 \times 10^{-9}$) in the rate of BMs relative to the random spatial distribution. A nonstochastic spatial distribution of metastases may be used to guide partial brain radiotherapy with risk-adapted dose delivery and reduce the risk of neurotoxicity due to overtreatment.

INTRODUCTION

Whole-brain radiotherapy (WBRT) for patients with brain metastases (BMs) is a commonly used technique to treat both visible and subclinical disease. Neurotoxicity is a major concern and protocols to reduce the volume of brain receiving a full dose are currently being tested in clinical trials. However, there are currently no available methods to risk-stratify regions of the brain on the basis of the probability of developing a BM. Accurate segmentation of the brain based on BM risk would permit the radiation dose to be spatially tailored to improve disease control in high-risk regions and spare neurotoxicity by reducing dose to low-risk regions.

More accurate radiation delivery has the potential of affecting numerous patients because BMs are the most common intracranial malignancy, with an annual incidence of >150 000 in the USA (1), and are diagnosed in ~10%–20% of patients with cancer (2, 3). Patients who have previously been treated for BMs or who are at an increased risk for developing BMs often undergo surveillance imaging with serial magnetic resonance imaging (MRI) scans, and treatment may involve focal radiotherapy, such as with stereotactic radiosurgery, or WBRT. Although WBRT remains the standard of care for many patients with BMs, improvements in systemic therapy have led to gains in survival for patients with metastatic disease, and the long-term neurocognitive toxicities associated with WBRT must now be weighed against the benefits of treatment. Therefore, several lines of investigation are now directed toward mitigating long-term toxicities associated with full-dose irradiation to the entire brain.

Partial brain techniques have recently been tested in an effort to reduce late neurocognitive decline that is associated with WBRT. RTOG 09-33 was a phase II study using intensity-modulated radiation therapy (IMRT) to selectively spare the hippocampi bilaterally while delivering a full dose to the remainder of the brain (4). Results showed that neurocognitive toxicities improved with IMRT relative to standard WBRT. In sparing the hippocampi from radiation toxicity, one would assume that patients would then be at an increased risk of developing metastatic foci in regions receiving a low radiation dose. On the contrary, local control appears to be maintained with IMRT, and extensive interrogation of the hippocampi revealed that it is at a very low risk for developing BMs (5). The finding that a critical brain structure can be safely spared the damaging effects of high-dose irradiation without compromising efficacy is intriguing and motivates investigation into other areas that might be at a low risk of developing BMs. Some studies have reported that the distribution of BMs may be based on the vasculature (6-8), but others have found that the pattern of spread is influenced by other factors, such as disease histology (9). The majority of the published work has relied on broad classifications of the brain, and there are currently no accepted atlases that segregate brain regions based on the risk of developing BMs.

Here, we hypothesized that discrete brain regions are involved with metastatic lesions beyond that which would be expected by chance. To test this, we identified 150 BMs in 28 patients treated at a single institution and compared the BMs'

ISSN 2379-1381 http://dx.doi.org/10.18383/j.tom.2016.00268

spatial distribution with a computer model of randomly distributed BMs. All BMs were coded by their voxel coordinates, and these were mapped onto 52 anatomical locations based on a common brain atlas to determine if particular regions were at increased risk of harboring metastatic disease.

METHODOLOGY

All procedures described in this study were approved by the institutional review board of Columbia University. We searched a database of patients with BMs from a primary diagnosis of either lung or breast cancer treated at our institution between December 2008 and January 2016 and selected those who met the following criteria: (1) were treated for at least 1 recurrent BM, (2) review of radiology reports determined that the BM recurrence was not definitively seen on a prior scan, and (3) all MRI data were available for analysis. Imaging data were obtained on either a 1.5 T or 3 T magnetic resonance scanner (GE Medical Systems Waukesha, Wisconsin) or a 1.5 T or 3 T magnetic resonance scanner (Philips Healthcare, Best, The Netherlands). Image processing was performed with the Functional MRI of the Brain Software Library (10) (FSL; Oxford, UK) and Matlab (MathWorks, Natick, Massachusetts). Brain extraction was performed for each imaging sequence. All brain lesions were manually contoured based on T1 contrast-enhanced scans.

T1 contrast-enhanced scans were coregistered using an affine registration (12 degrees of freedom) to the Montreal Neurological Institute (MNI) standard brain. Registration matrices were then applied to each manually contoured BM, and the center of gravity was computed to identify the centroid voxel, which was used as the "origin" of the BM. All voxel coordinates were maintained in MNI-space. The Harvard–Oxford cortical and subcortical (http://www.cma.mgh.harvard.edu/) atlases were used to determine the anatomical structures corresponding to each metastatic centroid. After removing ventricular spaces, broad anatomic boundaries that overlapped with other areas (eg, "cerebral cortex"), and combining subdivisions of particular regions (eg, "anterior" and "posterior" divisions), 52 anatomically defined regions of interest (ROIs) were included in our analyses (Figure 1).

Coordinates for each of the 150 observed BM centroids were mapped onto the atlas, and the frequency of involvement for all 52 ROIs was computed. This observed value was compared with the expected value, which assumed that each voxel within the brain was at an equal risk of being involved with a BM. Therefore, the probability of 1 of the 52 ROI harboring a BM was a function of that region's volume relative to the total volume of all 52 regions. The observed and expected rates of BMs for each ROI were compared with proportional 2-tailed hypothesis testing, which is presented as follows:

$$z = \frac{\hat{p} - p_0}{\sqrt{\frac{p_0(1-p_0)}{n}}}$$

$\hat{p}$: proportion of observed BMs
p_0: proportion of expected BMs
n: number of observed BMs
Z: z − score

Raw z-scores and *P*-values are reported, but we subjected the interpretation of all results to a Bonferroni correction to adjust for multiple comparisons across the 52 anatomic ROIs. There-

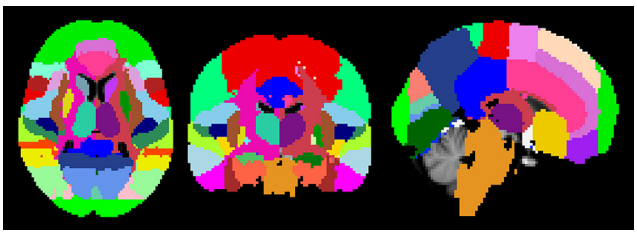

Figure 1. The Harvard–Oxford cortical brain atlas overlying the subcortical atlas and standard Montreal Neurological Institute (MNI) brain. In total, 52 distinct brain regions from the atlas were included in the analysis.

Table 1. Patient Characteristics and Additional Information for the 150 BMs Detected in this Cohort

Characteristic	No. of Patients (%)
Age (years)	
Mean	59.5
Range	38–89
Gender	
Male	11 (39)
Female	17 (61)
Histology	
Lung	19 (67.9)
EGFR+	5 (26.3)
KRAS+	2 (10.5)
ALK+	1 (5.3)
Breast	9 (32.1)
ER+, PR+, Her2−	2 (22.2)
ER+, PR+, Her2+	2 (22.2)
ER+, PR−, Her2+	1 (11.1)
ER−, PR+, Her2−	1 (11.1)
ER−, PR−, Her2+	2 (22.2)
ER−, PR−, Her2−	1 (11.1)
Lesions per patient	
Median	3
Range	1–19
Lesion volume (cc)	
Mean	1.196
Range	0.128–18.368
Initial treatment	
Resection and adjuvant SRS	14 (50)
SRS alone	11 (39.3)
WBRT	3 (10.7)

Abbreviations: eGFR, estimated glomerular filtration rate; SRS, stereotactic surgery; WBRT, whole-body radiation therapy; No., number.

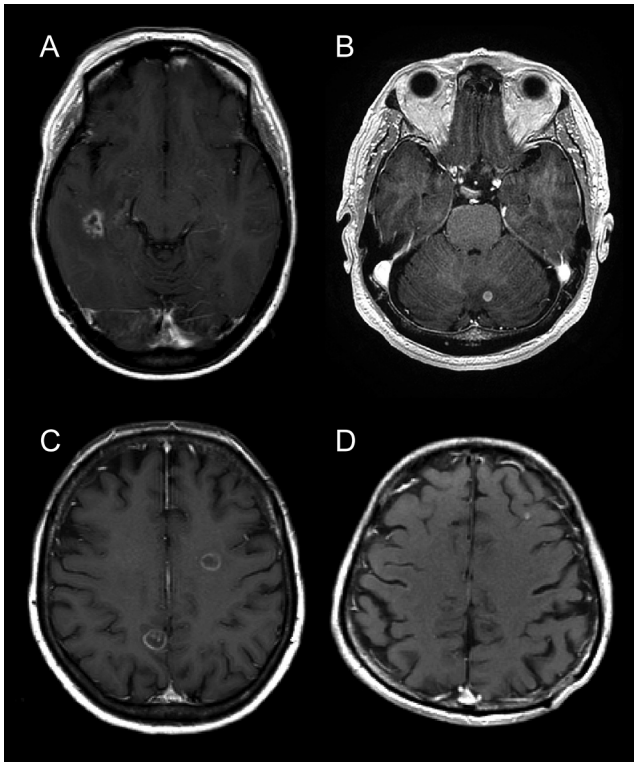

Figure 2. Representative axial T1 contrast-enhanced images from 4 patients were included in the analysis. A large ring-enhancing lesion in the right middle temporal lobe in the posterior insular cortex represents metastatic breast cancer (A). In another patient, a small enhancing metastatic focus from non-small cell lung cancer (NSCLC) can be appreciated in the medial left cerebellum (B). A patient with multifocal recurrent BMs from a primary NSCLC is also shown where 2 large ring-enhancing lesions are seen on the same axial section (C). Finally, a small enhancing nodule from a metastatic breast cancer is visualized in the left frontal lobe (D).

fore, the *P*-value needed to reach statistical significance was $P \leq 9.804 \times 10^{-4}$.

RESULTS

There were 11 (39%) male and 17 (61%) female patients identified with a primary cancer diagnosis of non-small cell lung cancer in 19 (68%) and breast cancer in 9 (32%) patients (Table 1). The mean age of all patients was 59.5 years (range, 38–89 years). The mean volume of all BMs was 1.196 cc (range, 0.128–18.368 cc). Several representative BMs are depicted in Figure 2 from 4 patients included in the analysis.

To visually inspect all BMs, a 3-dimentional rendering was created with all 150 lesions projected onto the MNI brain and dilated to the median BM diameter (see Supplemental Video PLAY VIDEO). The 3-dimensional rendering provides a qualitative evaluation of spatial variations in BM distribution. To test for a nonstochastic spatial distribution, we compared the observed with the expected rate of BMs for each ROI. In this approach, the null hypothesis is that the spatial distribution of BMs is stochastic and the probability of detecting a BM within a brain region is a function of that region's volume.

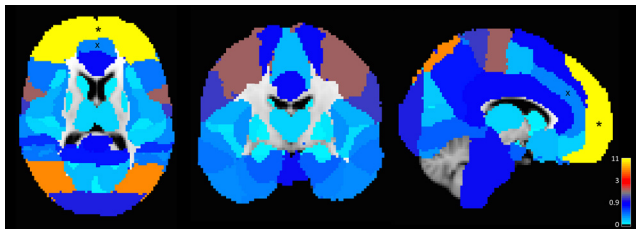

Figure 3. Classification of all 52 regions of interest (ROIs) included in the analysis by their proportional volume relative to the entire area at risk for developing a BM. Each region's color corresponds to the percent of the total volume as labeled by the colorbar (bottom right). For example, the fontal pole (*, bright yellow) contained the largest number of voxels, making up 11% of the total volume for all 52 ROIs. The paracingulate cortex (x, light blue) consists of a relatively small proportional volume at 1.7% of the total volume analyzed.

For each of the 52 brain regions, 2 parcellations were performed. First, each atlas-based region was coded by its proportional volume relative to all 52 ROIs (Figure 3). Second, within each region, voxels were coded by the number of BMs observed in the

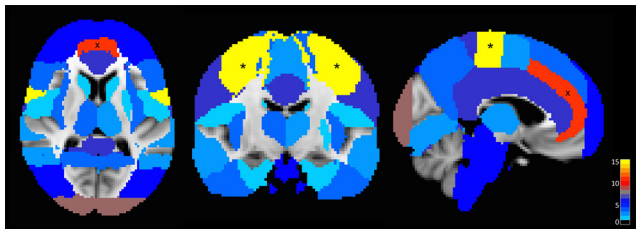

Figure 4. Cortical and subcortical anatomic brain regions as defined by the Harvard–Oxford atlas are color coded by the number of brain metastases detected within the anatomic boundaries from the 150 lesions analyzed. In total, 20 lesions fell outside the bounds of any of the 52 ROIs, leaving 130 BMs to be analyzed. The area with the highest frequency of involvement was the precentral gyrus (*, bright yellow), which was affected by 15 metastases, which was not significantly increased above the predicted value after correction for multiple comparisons. The paracingulate gyrus (x, red) contained 11 lesions, which was the only ROI that was significantly increased above the expected rate after Bonferroni correction.

Table 2. Results from the Analysis for all 52 ROIs

Atlas Region	Volume (cc)	% Volume at Risk	No. Observed	Observed Rate	z-Score	*P*-Value
Angular gyrus	29.624	0.016	3	0.023	0.671	.502
Brain stem	72.376	0.039	5	0.039	−0.001	.999
Central opercular cortex	20.624	0.011	1	0.008	−0.358	.720
Cingulate gyrus	70.496	0.038	6	0.046	0.521	.603
Cuneal cortex	13.944	0.007	0	0	−0.985	.324
Frontal medial cortex	12.312	0.007	0	0	−0.926	.355
Frontal operculum cortex	8.496	0.005	0	0	−0.768	.442
Frontal orbital cortex	41.504	0.022	6	0.046	1.869	.062
Frontal pole	207.200	0.110	5	0.039	−2.611	.009
Heschl's gyrus	6.288	0.003	0	0	−0.660	.509
Inferior frontal gyrus	37.216	0.020	3	0.023	0.269	.788
Inferior temporal gyrus	64.240	0.034	3	0.023	−0.696	.487
Insular cortex	28.904	0.015	3	0.023	0.715	.475
Intracalcarine cortex	17.688	0.009	0	0	−1.111	.267
Lateral occipital cortex	175.792	0.094	5	0.039	−2.155	.031
Left accumbens	0.712	0.000	0	0	−0.222	.824
Left amygdala	2.656	0.001	0	0	−0.429	.668
Left caudate	3.896	0.002	1	0.008	1.410	.159
Left hippocampus	6.120	0.003	0	0	−0.652	.515
Left pallidum	2.136	0.001	0	0	−0.385	.701
Left putamen	6.392	0.003	1	0.008	0.841	.400
Left thalamus	11.760	0.006	2	0.015	1.321	.187
Lingual gyrus	43.104	0.023	2	0.015	−0.574	.566
Middle frontal gyrus	67.368	0.036	9	0.069	2.050	.040
Middle temporal gyrus	70.664	0.038	2	0.015	−1.330	.183
Occipital fusiform gyrus	28.696	0.015	6	0.046	2.874	.004
Occipital pole	77.264	0.041	8	0.062	1.175	.240
Paracingulate gyrus	32.760	0.017	11	0.085	5.856	4.731×10^{-9}
Parahippocampal gyrus	42.616	0.023	1	0.008	−1.147	.252
Parietal operculum cortex	13.472	0.007	2	0.015	1.112	.266
Planum polare	9.680	0.005	0	0	−0.820	.412
Planum temporale	11.536	0.006	0	0	−0.896	.370
Postcentral gyrus	85.104	0.045	6	0.046	0.050	.960
Precentral gyrus	111.736	0.059	15	0.115	2.700	.007
Precuneous cortex	62.752	0.033	3	0.023	−0.653	.514
Right accumbens	0.672	0.000	0	0	−0.216	.829
Right amygdala	3.304	0.002	0	0	−0.478	.632
Right caudate	4.088	0.002	1	0.008	1.351	.177
Right hippocampus	6.120	0.003	0	0	−0.652	.515
Right pallidum	2.080	0.001	0	0	−0.379	.704
Right putamen	6.368	0.003	0	0	−0.665	.506
Right thalamus	11.208	0.006	3	0.023	2.536	.011
Subcallosal cortex	17.408	0.009	0	0	−1.102	.270
Superior frontal gyrus	70.888	0.038	3	0.023	−0.875	.382

(Continued)

Table 2. Continued

Atlas Region	Volume (cc)	% Volume at Risk	No. Observed	Observed Rate	z-Score	*P*-Value
Superior parietal lobule	35.912	0.019	3	0.023	0.332	.740
Superior temporal gyrus	30.504	0.016	2	0.015	−0.075	.940
Supplementary motor cortex	18.256	0.010	2	0.015	0.660	.509
Supracalcarine cortex	3.392	0.002	0	0	−0.485	.628
Supramarginal gyrus	55.848	0.030	0	0	−1.995	.046
Temporal fusiform cortex	33.552	0.018	3	0.023	0.451	.652
Temporal occipital Fusiform cortex	19.664	0.011	4	0.031	2.277	.023
Temporal pole	64.352	0.034	0	0	−2.146	.032
Total	**1880.744**	**1**	**130**	**1**	**—**	**—**

The percent volume at risk (column three) is the volume of the individual brain region divided by the volume of all 52 analyzed ROIs. This was used to determine the expected number of BMs assuming a stochastic distribution. The number of BMs observed in the cohort of patients within each ROI and the fraction of the total analyzed are also reported (columns 4 and 5, respectively). Proportional hypothesis testing was used to compute a z-score and 2-tailed *P*-value. The reported *P*-values were not corrected for multiple comparisons, and a Bonferroni correction yielded an $\alpha \leq 9.804 \times 10^{-4}$. Highlighted rows indicate ROIs with a *P*-value of ≤.05. No., number.

cohort of 150 lesions that fell within that ROI (Figure 4). We noted that 21 lesions fell outside the bounds of any ROI identified in the atlas. Therefore, the final analysis consisted of 130 observed BMs. An increased frequency of BMs can be appreciated along the major branches of the anterior cerebral artery in the region of the paracingulate (ie, precingulate) gyrus. There also appears to be a general increase in the frequency of BMs in superficial rather than deep brain structures.

The frequency of BMs observed was significantly different from the expected value in 10 ROIs at $P \leq .05$ and 4 ROIs at $P \leq .01$ (Table 2). Only the paracingulate gyrus reached significance after a Bonferroni correction for multiple comparisons (Figure 5). Four regions: frontal pole, lateral occipital cortex, supramarginal gyrus, and temporal pole, had fewer observed BMs that were predicted by the simulation, with *P*-values of .009, .031, .046, and .032, respectively. The possibility that this is an artifact of having a relatively small sample size of observed lesions cannot be ruled out from these data. Similarly, of the 52 anatomically defined brain regions in the atlas, 20 were not observed to have a BM, and this was likely influenced by the small sample size. We note that, consistent with the low rate of observed metastases in these ROIs, these 20 regions made up a small fraction of the total volume at risk (13.35%) with an average proportional volume of 0.67% (range, 0.04%–3.42%).

Finally, because the hippocampus has been the subject of prior investigations quantifying the frequency of BM involvement, we specifically reviewed results for this ROI. A review of the bilateral hippocampi and parahippocampal gyrus revealed that only 1 of the 150 total BMs in the cohort could be identified in the area. This is consistent with the literature, which has shown a near-zero rate of BM involvement with this structure (5, 6, 11).

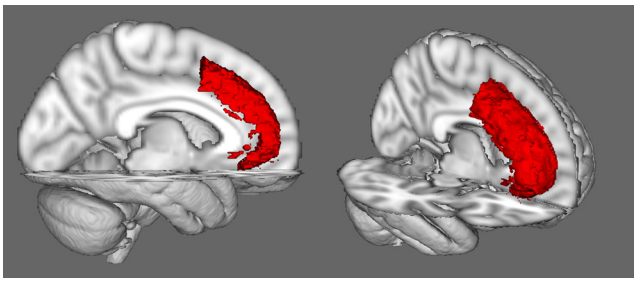

Figure 5. Three-dimensional visualization of the paracingulate cortex (red). The region makes up a relatively small fraction of the total volume of brain tissue analyzed (1.7%), and it is notable for its close proximity to major vessels of the anterior cerebral circulation.

DISCUSSION

Metastatic disease may develop anywhere within brain, but it may have a nonrandom distribution that has not previously been quantified. Here, we hypothesized that the spatial frequency of BMs follows a nonstochastic distribution. To test this, we identified 150 BMs in 28 patients treated at a single institution and used the major divisions of the Harvard–Oxford cortical and subcortical atlases to identify anatomic regions that were involved. We then compared these values with the expected rates under the assumption that all voxels were at equal risk and that the probability of a brain region being affected by a metastatic focus was a function of the region's volume. Ten regions within the atlas showed a significantly different number of BMs that would be expected by chance, and the paracingulate cortex maintained significance after correction for multiple comparisons.

These results may be used to develop automated techniques to identify BMs where the nonuniform spatial distribution of these lesions could be used as *a priori* information to improve search algorithms. Of more immediate clinical relevance is the influence of our results on partial brain radiotherapy.

Prior investigations have showed a tendency for metastases to develop at terminal branches of arteries at gray–white boundaries

and possibly at watershed areas (11, 12). Additional work has revealed variations in BM distribution across the supra- and infratentorial brain. In 1 study, ~70%–80% of lesions were identified in the cerebral hemispheres, 15%–20% in the cerebellum, and ≤3% in the brainstem, which are thought to roughly follow patterns of blood flow (6-8). Contrary to these results, a detailed autopsy analysis identified nearly equivalent rates of BM involvement in the cerebellum as compared with the cerebrum (9). One explanation for the varying results may be differential patterns of BM distribution based on the primary histology or may be an artifact of how finely the cerebrum is segmented.

Bender and Tome provided the first analysis to help inform this debate by using atlas-based brain segmentation and stratifying BMs by the histology of the primary cancer (13). This revealed that lung and breast cancer might have a predilection for the cerebellum, which aligns with prior autopsy results (9). The authors further show the potential for these data to influence BM treatment, where a nonuniform dose distribution may improve tumor control probability. These studies have provided insight into the pathophysiology of BMs, but have provided a broad description of BM distribution without an analysis of individual cortical and subcortical regions. A more granular understanding of BM distribution may permit sparing of additional brain regions with partial brain radiotherapy to further improve the therapeutic window.

A recently completed national clinical trial, RTOG 09-33 (NCT01227954), showed a reduction in neurocognitive toxicities associated with whole-brain irradiation for BM when the hippocampi were avoided (4). The rationale for sparing the hippocampus to spare side effects is bolstered by the finding that the area is at relatively low risk for developing BMs. Detailed analyses have been performed to assess the risk for failure within the hippocampi plus a margin. These studies have estimated that between 0% and 0.4% of BMs are located within the hippocampus and ~3% are within 5 mm of the hippocampus (5, 6, 14). This is considered an acceptably low risk and has allowed for IMRT to be used. In contrast to traditional whole-brain irradiation, IMRT allows for variable dose prescriptions to be delivered across the brain.

The success of RTOG 0933 has motivated additional studies, and partial brain techniques to spare the hippocampi are now being tested in numerous clinical trials. These include NRG-CC001, a phase III trial evaluating the role of memantine and brain irradiation with or without hippocampal avoidance (NCT02360215), and NRG-CC003 (NCT02635009), a phase II/III trial also comparing whole-brain treatment with or without hippocampal sparing in the setting of prophylactic cranial irradiation for small cell lung cancer. In addition to sparing particular brain areas, IMRT has the potential to ensure that high-risk regions receive adequate coverage or dose-escalated radiation. However, to the best of our knowledge, no ongoing trial uses any form of advanced radiation planning for this purpose. Tools to segment brain regions based on the rate of BM development would allow risk-based IMRT dosing to further improve the therapeutic window.

In the current study, patients with recurrent BMs were chosen because this is the population that may benefit from risk-adapted treatment with WBRT. For example, if a patient with BMs requires treatment for a low volume of disease and there is an opportunity to treat the brain partially, radiation may be tailored to avoid regions that are at a low risk of developing subsequent lesions. An additional rationale for analyzing patients with recurrent BMs is that this population is under close imaging surveillance, which typically identifies BMs when they are small and can be correlated to a specific anatomical focus. The selection of this patient population excludes those who have a cancer diagnosis, but do not have known brain involvement. Therefore, there may be limited application of these findings to patients being considered for prophylactic cranial irradiation, such as select patients with small cell lung cancer.

Another limitation of this study is the relatively small sample size of the clinically defined BMs. Although this does not challenge the interpretation that the paracingulate gyrus is at an increased risk of BM involvement, this may subject the study to more type II error. Further, the use of a stringent Bonferroni correction may further increase the false negative rate, but it strengthens the claim regarding the paracingulate gyrus. Therefore, it is likely that other brain regions are also at a relatively increased risk of developing BMs, and our data suggest that the paracingulate gyrus is among the most at-risk regions. To validate the findings of this study, reduce type II error, and improve applicability to other patient populations, future work should include a greater number of BMs and other histologies.

Supplemental Materials

Supplemental Video: http://dx.doi.org/10.18383/j.tom.2016.00268.vid.01

ACKNOWLEDGMENTS

This publication was supported by the National Center for Advancing Translational Sciences, National Institutes of Health (NIH), through Grant Number UL1 TR000040. The content is solely the responsibility of the authors and does not necessarily represent the official views of the NIH. The authors thank Dr. Jack Grinband and Samuel Heilbroner for their thoughtful contributions to this work.

Disclosures: No disclosures to report.

REFERENCES

1. Ewend MG, Morris DE, Carey LA, Ladha AM, Brem S. Guidelines for the initial management of metastatic brain tumors: role of surgery, radiosurgery, and radiation therapy. J Natl Compr Canc Netw. 2008;6(5):505–514.
2. Garrett MD WC, Yanagihara TK, Jani A, Wang TJC. Radiation therapy for the management of brain metastases. Am J Clin Oncol. 2016;39(4):416–422.

3. Lin X, DeAngelis LM. Treatment of brain metastases. J Clin Oncol. 2015;33(30): 3475–3484.
4. Gondi V, Pugh SL, Tome WA, Caine C, Corn B, Kanner A, Rowley H, Kundapur V, DeNittis A, Greenspoon JN, Konski AA, Bauman GS, Shah S, Shi W, Wendland M, Kachnic L, Mehta MP. Preservation of memory with conformal avoidance of the hippocampal neural stem-cell compartment during whole-brain radiotherapy for brain metastases (RTOG 0933): a phase II multi-institutional trial. J Clin Oncol. 2014;32(34):3810–3816.
5. Gondi V, Tome WA, Marsh J, Struck A, Ghia A, Turian JV, Bentzen SM, Kuo JS, Khuntia D, Mehta MP. Estimated risk of perihippocampal disease progression after hippocampal avoidance during whole-brain radiotherapy: safety profile for RTOG 0933. Radiother Oncol. 2010;95(3):327–331.
6. Ghia A, Tomé WA, Thomas S, Cannon G, Khuntia D, Kuo JS, Mehta MP. Distribution of brain metastases in relation to the hippocampus: implications for neurocognitive functional preservation. Int J Radiat Oncol Biol Phys. 2007;68(4):971–977.
7. Haar F, Patterson RH Jr. Surgery for metastatic intracranial neoplasm. Cancer. 1972;30(5):1241–1245.
8. Gavrilovic IT, Posner JB. Brain metastases: epidemiology and pathophysiology. J Neurooncol. 2005;75(1):5–14.
9. Tsukada Y, Fouad A, Pickren JW, Lane WW. Central nervous system metastasis from breast carcinoma. Autopsy study. Cancer. 1983;52(12): 2349–2354.
10. Jenkinson M, Beckmann CF, Behrens TE, Woolrich MW, Smith SM. FSL. Neuroimage. 2012;62(2):782–790.
11. Hwang TL, Close TP, Grego JM, Brannon WL, Gonzales F. Predilection of brain metastasis in gray and white matter junction and vascular border zones. Cancer. 1996;77(8):1551–1555.
12. Delattre JY, Krol G, Thaler HT, Posner JB. Distribution of brain metastases. Arch Neurol. 1988;45(7):741–744.
13. Bender ET, Tomé WA. Distribution of brain metastases: implications for non-uniform dose prescriptions. Br J Radiol. 2014;84(1003):649–658.
14. Harth S, Abo-Madyan Y, Zheng L, Siebenlist K, Herskind C, Wenz F, Giordano FA. Estimation of intracranial failure risk following hippocampal-sparing whole brain radiotherapy. Radiother Oncol. 2013;109(1):152–158.